Magnetization Transfer MRI in Pancreatic Cancer Xenograft Models

Weiguo Li[1], Zhuoli Zhang[1], Jodi Nicolai[1], Guang-Yu Yang[2], Reed Omary[1], and Andrew Larson[1]
[1]Radiology, Northwestern University, Chicago, IL, United States, [2]Pathology, Northwestern University, Chicago, IL, United States

INTRODUCTION Tumor desmoplasia, the remarkable growth of fibrotic connective tissue, is a common hallmark of pancreatic ductal adenocarcinoma (PDAC), the 4th leading cause of cancer-related mortality [1]. Recent studies clearly indicate that desmoplasia actively facilitates disease progression, metastasis, and drug resistance [2]. Precise quantification of tumor fibrosis levels in PDAC may be critically important for patient staging and for the prediction or monitoring of responses to therapy. The current gold-standard for characterizing desmoplasia—histologic analysis of biopsy samples—is invasive and cannot avoid misrepresentation by reason of sampling error. Therefore, new methods to permit noninvasive quantification of fibrosis levels in PDAC would be particularly useful. Diffusion-weighted MRI and dynamic contrast enhanced (DCE) MRI methods can detect alterations to PDAC [3, 4] but the development of quantitative imaging metrics independent of perfusion levels may be valuable for desmoplasia assessment in PDAC. Magnetization transfer (MT) MRI can be used to non-invasively probe dynamic physical processes involving the exchange of magnetization between sub-populations of free water protons and those water protons bound to tissue macromolecules [5]. MT-MRI studies have demonstrated that MT contrast (MTC) can be highly sensitive to tissue collagen concentration [6], the primary component of desmoplasia. Thus, we hypothesized that desmoplasia-associated fibrosis levels in PDAC may be directly reflected in MT-MRI magnetization transfer ratio (MTR) measurements. The purpose of this study was to compare non-invasive MTR measurements to invasive histologic assessments of tumor fibrosis-levels in three mouse xenograft models of PDAC.

MATERIALS AND METHODS

Mouse Xenograft Models Three cell lines (Panc-1, BxPC-3, and Capan-1 from ATCC) were cultured and implanted to each flank (5×10^6 cells in 200 µL PBS) of Six-week-old nude mice (Balb/c mice) from Charles River (Wilmington, MA). 21 days following tumor implantation, mice were anesthetized for MRI scans. All animal studies were approved by an Institutional Animal Care and Use Committee. ***MR Imaging*** MRI studies were performed using a 7 T, 16 cm bore size Bruker Pharmascan system with a 72 mm volume coil transmitter and a 38 mm mouse coil receiver (Bruker BioSpin, Billerica, MA). A 3D spoiled gradient echo pulse sequence (TR/TE/flip-angle = 36/2.93/9°) with a 20 ms, 8 µT Gaussian RF pulse applied 3.5 kHz off-resonance was used to generate MTC. The same Gaussian pulse with an off-resonance frequency of 100 kHz was applied to generate MR images without MT saturation. Additional imaging parameters included: FOV = 32×32 mm^2; slab thickness = 16 mm; matrix = 128 × 128 × 16; NEX = 2. ***Histology*** Each tumor was fixed, embedded, and sliced (4 µm slice thickness). The trichrome-stained slides (one central slice from each tumor) were scanned at 20× magnification and digitized using TissueFAXS system (TissueGnostics, Los Angeles, CA). HistoQuest Software (TissueGnostics, Los Angeles, CA) was then used for automated measurement of the fibrotic tissue areas within each slide ($A_{fibrosis}$, distinct blue regions defined as the fibrotic tissue area) and the total tumor tissue area (A_{total}). The percentage of fibrotic tissue was expressed as a ratio of the latter two area measurements: $A_{fibrosis} / A_{total} \times 100$. ***Data Analysis*** All post processing was performed offline using Matlab software (MathWorks, Natick, MA). Voxel-wise MTR maps were calculated as follows: $100 \times (1 - M_{sat} / M_0)$, where M_{sat} represents the signal intensity for image acquired following application of the MT pulse, and M_0 is the signal intensity for image acquired without MT saturation. For imaging slice through the center of each tumor, a region-of-interest (ROI) was drawn to circumscribe the entire tumor (identical ROIs were transferred to M_{sat} and M_0 images as well as corresponding MTR maps); the mean MTR value was reported for each tumor. One-way analysis of variance (ANOVA) was used to compare MTR measurements and fibrotic area measurements for the xenograft tumors grown from each of the three PDAC cell lines. Pearson correlation coefficients were calculated to assess the relationship between MTR measurements and corresponding histologic fibrosis measurements. All statistical analyses were performed with Stata software (Stata11, Stata-Corp, College Station, Tex).

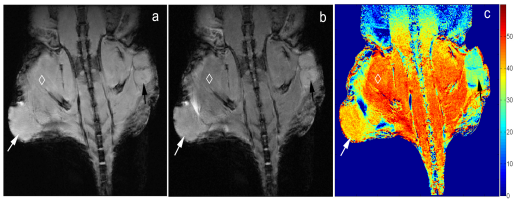

Fig.1. Coronal MR images without (a) and with MT (b) of a mouse with BxPC-3 tumor in right flank, Panc-1 tumor in left flank and corresponding MTR maps (c).

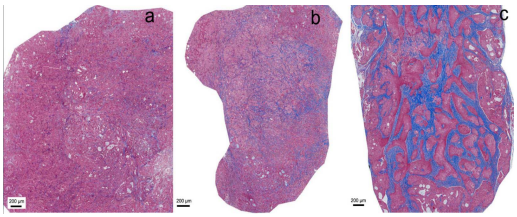

Fig.2. Masson-trichrome stained histology slices from tumors grown using each of the three PDAC cell lines: (a) Capan-1, (b) Panc-1 and (c) BxPC-3.

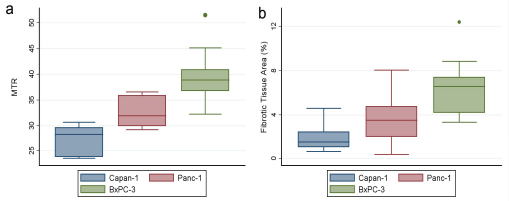

Fig.3. Box-and-Whisker plots for MTR (a) and histologic fibrotic tissue area (b) measurements for each of the three cell lines.

RESULTS A total of 28 PDAC xenografts were grown in the 14 mice with 10 tumors from Panc-1 cell line, 11 tumors from BxPC-3 cell line and 7 tumors from Capan-1 cell line. Representative MT images and corresponding MTR maps for one mouse are shown in **Fig. 1**. The tumor in the right flank (white arrow) was grown from the BxPC-3 cell line and demonstrated markedly higher MT effects (39.78 ± 2.84) compared to the left flank tumor (black arrow) grown in the same animal but using the Panc-1 cell line (30.19 ± 3.08, **Fig. 1c**). Representative tri-chrome histology slides for Capan-1, Panc-1, and BxPC-3 xenograft tumors are shown in **Fig. 2**. These slides clearly depict the fibrotic stroma seen histologically as blue-stained bands of collagen enveloping the tumor cells in each xenograft. A summary of both our in vivo MTR measurements and histologic measurements of fibrotic tissue area for each tumor type is shown in **Fig. 3**. MTR measurements from the 11 tumors grown from the BxPC-3 cell line (39.4 ± 5.1) were higher than MTR measurements in 10 tumors grown from Panc-1 cell line (32.4 ± 2.8) and the 7 tumors from Capan-1 cell line (27.3 ± 2.8), **Fig. 3a**. BxPC-3 MTR measurements were significantly different compared to both Panc-1 and Capan-1 measurements ($P = 0.001$ and < 0.000, respectively); a significant difference was also found between MTR measurements in Panc-1 and Capan-1 xenografts ($P = 0.038$). Histologic trichrome measurements showed a similar trend (**Fig. 3b**) with tumors grown from the BxPC-3 cell line demonstrating significantly higher fibrotic areas (percentage fibrosis area, 6.48 ± 2.59) when compared to Panc-1 fibrotic areas (3.54 ± 2.18) and Capan-1 (2.07 ± 1.60), respectively. BxPC-3 fibrotic tissue area measurements were significantly higher when compared to both Panc-1 and Capan-1 measurements ($P = 0.014$ and 0.001, respectively); A direct comparison of MTR measurements to corresponding histologic fibrotic area measurements across all tumor types further illustrated these relationships ($r = 0.69$, $P = 0.01$; **Fig. 4**).

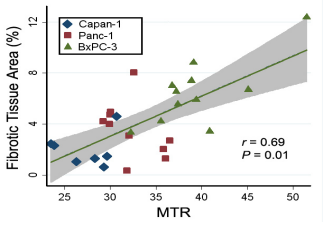

Fig.4. Relationship between MTR and histologic measurements.

DISCUSSION Resulting MTR measurements in this study were significantly different for these three tumor models and corresponding histology measurements demonstrated significantly different fibrosis levels for each tumor type. Further translational studies remain necessary to validate the efficacy of these methods in clinical patients but these initial encouraging results strongly suggest the feasibility of using MTR measurements as a non-invasive biomarker of tumor associated desmoplasia in PDAC.

REFERENCE [1] Jemal A et al. CA Cancer J Clin 2008;58(2):71-96. [2] Olive K et al. Science 2009; 324:1457-61. [3] Muraoka N et al. J Magn Reson Imaging. 2008 27:1302-8. [4] Watanabe H, et al. Radiology 2011;259(1):142-150. [5] Henkelman R et al. MRM 1993; 29(6):759-66. [6] Adler J et al. Radiology 2011; 259(1):127-35.

ACKNOWLEDGEMENTS: The authors wish to acknowledge the support of NIH grant RO1 CA134719, ACS SP001149, and NUCATS grant UL1RR025741.